Peer-reviewed version available at Electronics 2019, 8, 1217; doi:10.3390/electronics8111217

Article

Characterization and Correction of the Geometric Errors in Using Confocal Microscope for Extended Topography Measurement. Part II: Experimental Study and Uncertainty Evaluation

Chen Wang[1], Emilio Gómez[1] and Yingjie Yu[2,*]

[1] Department of Mechanical Engineering, Chemical and Industrial Design, ETS of Engineering and Industrial Design, Technical University of Madrid, Madrid, 28012, SpainCity Post Code, Country ; chen.wang@alumnos.upm.es (C.W.); emilio.gomez@upm.es (E.G.)

[2] Department of precision mechanical engineering, Shanghai University. No.333, Nanchen Rd., Shanghai, 200444

* **Correspondence:** yingjieyu@staff.shu.edu.cn

Abstract: This paper presents the experimental implementations of the mathematical models and algorithms developed in Part I. Two experiments are carried out. The first experiment aims at the determinations of the correction coefficients of the mathematical model. The dot grid target is measured and the measurement data are processed by our developed and validated algorithms introduced in Part I. The values of the coefficients are indicated and analysed. Uncertainties are evaluated with implementation of the Monte Carlo method. The second experiment measures a different area of the dot grid target. The measurement results are corrected according to the coefficients determined in the first experiment. The mean residual between the measured points and their corresponding certified values reduced 29.6% after the correction. The sum of squared errors reduced 47.7%. The methods and the algorithms for raw data processing, such as data partition, fittings of dots' centres, K-means clustering, etc., are the same for both two experiments. The experimental results demonstrate that our method for the correction of the errors produced by the movement of lateral stage of confocal microscope is meaningful and practicable.

Keywords: Geometric errors**;** rigid body kinematics**;** lateral stage errors**;** Imaging Confocal Microscope**;** MCM uncertainty evaluation**;** dot grid target.

1. Introduction

The increasing demands for manufacturing accuracies and quality control due to the rapid development of nanotechnology, ultraprecision machining, micro- and nano-fabrications, etc. [1, 2] and the requirements for precision in surface finishing in different technologies such as additive manufacturing [3], mechanical parts with structured surfaces [4], etc., require the use of increasingly sophisticated measurement systems and measurement traceability from a metrological point of view.

Calibration provides wide range information of the microscope performances. The ever increasing demand for improved surface quality and tighter geometric tolerances leads to the augmentations in the investigations of manufacturing technologies [5]. Measurements using optical microscopes are often affected by common path noise, disturbance in light source and ambient lighting, etc., causing measurement defects and outliers 6, 7] as well as attracting investigations on noisy data processing [8] The need for standardization is becoming ever greater as the range of capturing 3D information of microscope techniques continues to increase [5, 9]. For optical confocal microscopes, the Z-calibrations at nm-levels are typically good while the X- and Y- accuracies are often left without further notice than resolution limits of the optics [10, 11]. Among the

investigations of the lateral calibrations, lots of studies focus on its optical system [**Error! Reference source not found.**]. For example, H. Ni, *et al*. proposed a new method to achieve structured detection through using spatial light modulator, which modulates the Airy disk amplitude distribution according to the detection function in collection arm [13]; B. Wang, *et al.* presented confocal microscopy with structured detection in a coherent imaging process to achieve a higher resolution with a comparably large pinhole [14]. However, the systematic geometric errors which adversely affect the relative position and orientation between measuring probes and measurands are usually neglected [15, 16]. B. Daemi, *et al.* designed a comprehensive verification test by using a high precision metrology method based on subpixel resolution image analysis [17]. Calibration of confocal microscopes usually relies on traceable standard artefacts, which are commonly made up of regular patterns [10].

This paper carries out the experimental studies based on the kinematic modelling and algorithms for the correction of the geometric errors developed in Part I [18]. Sections 2 and 3 introduce the methodologies for experiments and uncertainty evaluation individually. Section 4 presents the experiment on a dot grid target for correction coefficients determination and their corresponding uncertainty evaluation. Section 5 implements an experiment and corrects the measured data with determined coefficients, comparing the residuals with respect to certified values before and after corrections. Section 6 presents the conclusions. Acknowledgements and references are indicated in the final section.

2. Methodology for the experimental study

The experimental study aims at: First, determining the error correction coefficients, i.e. $a_1, a_2, ..., f_3$, defined in the kinematic geometric error correction model developed in Part I; Second, applying the determined parameters of coefficients and the correction mathematical model for new measurement data calibration. The dot grid target standard artefact is implemented as measurand of the experiments. By comparing the residuals of measured points and corrected points with respect to the certified values, the practicality and significance of our developed models and algorithms for lateral stage error calibration can be observed.

Two experiments are carried out with our Imaging Confocal Microscope, which type is Leica Confocal Dual Core 3D Measuring Microscope (Leica DCM-3D), at the "*Laboratorio de Investigación de Materiales de Interés Tecnológico*" (LIMIT) of the Technical University of Madrid. The first experiment is to measure the dot grid target standard for the determination of the correction coefficients. The second experiment measures another area of the dot grid standard, processing the measurement data with the same developed and validated algorithms implemented in the first experiment. The purpose of this experiment is to observe whether the corrected data improved comparing with the raw measurement data. As the second experiment uses the same measurement parameters, data processing algorithms and procedures, and measure different area of the same dot grid standard, this comparison means a lot as other factors which might influence the results could be excluded majorly, such as the uncertainties or inaccuracies generated by algorithms of cylinder separation, centre fitting, movement scope of the lateral stage, etc.

3. Methodology and procedures for uncertainty estimation

A statement of measurement is complete only if it provides an estimate of the quantity concerned as well as a quantitative evaluation of the estimate's reliability, i.e., the associated uncertainty [**Error! Reference source not found.**]. Accompany measurement results by quantitative statements about their accuracy is very important particularly when the result is part of a measurement chain tracking back to national standards or when decisions about product specifications are taken [**Error! Reference source not found.**].

The document issued by BIPM, *Guide to the Expression of Uncertainty in Measurement* (GUM) [21] provides a method and procedure for the evaluation and expression of measurement

uncertainties [22]. This method is termed as GUM uncertainty framework in supplement 1 and supplement 2 (GUM-S1 and GUM-S2) [23, 24] and other bibliographies [19, 20]. The GUM uncertainty framework has two main limitations [**Error! Reference source not found.**, 25]. The first limitation is lacking generality of the procedure to obtain an interval to contain the values of the measurand with a stipulated coverage probability [25]. In the GUM uncertainty framework the way a coverage interval is constructed to contain values of the measurand with a stipulated coverage probability is approximate [22]. The second limitation is that insufficient guidance is given for the multivariate case in which there is more than one measurand, namely, more than one output quantity [22, 25]. In order to address these limitations, Working Group 1 of the Joint Committee for Guides in Metrology (JCGM) has produced two specific guidance documents, namely GUM-S1 and GUM-S2 [23, 24] , on Monte Carlo method (MCM) respectively for uncertainty evaluation and extensions to any number of measurand (output quantity) [22].

MCM provides a general approach to obtain a numerical representation $\mathbf{G}$ of the distribution function $G_{\mathbf{Y}}(\boldsymbol{\eta})$ for $\mathbf{Y}$. The heart of the approach is making repeated draws from the Probability Density Functions (PDFs) for the input variables X_i (or joint PDF for $\mathbf{X}$) and the evaluation of the output quantity. Assignment of the PDFs for the input variables will be dependent on each experiment and be explained in the part of experimental studies. The same case applies to the evaluation of the output quantity. The distribution function $G_{\mathbf{Y}}(\boldsymbol{\eta})$ encodes all information known about the output quantity $\mathbf{Y}$. Properties of $\mathbf{Y}$ can be approximated using $G_{\mathbf{Y}}(\boldsymbol{\eta})$. The quality of $\mathbf{G}$ depends on the number of draws made. The symbol $\mathbf{y}$ represent the output measurement results. It is determined by the input measurement results $\mathbf{x}_i$:

$$\mathbf{y} = f(\mathbf{x}_1, ..., \mathbf{x}_N) \tag{1}$$

The relationship between the PDF of output measurement results and input measurement results is:

$$\mathbf{g}_{\mathbf{Y}}(\boldsymbol{\eta}) = \int \mathbf{g}_{\mathbf{X}_1,...,\mathbf{X}_N}(\xi_1, ..., \xi_N) \times \delta\left[\boldsymbol{\eta} - f(\xi_1, ..., \xi_N)\right] d\xi_1 ... d\xi_N \tag{2}$$

where $\boldsymbol{\eta}$ denotes possible values that can be distributed to $\mathbf{Y}$, $\delta[\cdots]$ denotes the Dirac delta function.

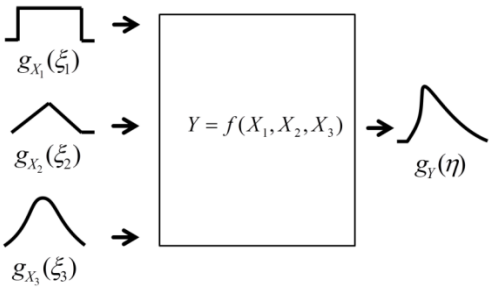

Figure 1. Illustration of the propagation of distributions for input quantities and the obtained output quantities [**Error! Reference source not found.**].

Figure 1 makes an illustration of the propagation of distributions for input and output quantities. The expectation of the output quantities can be obtained by its PDF $\mathbf{g}_{\mathbf{Y}}(\boldsymbol{\eta})$ as:

$$E(Y_i) = \int_{-\infty}^{\infty} \eta_i g_{Y_i}(\eta_i) d\eta_i \tag{3}$$

The variance of the output quantities can be obtained by its PDF $\mathbf{g}_{\mathbf{Y}}(\boldsymbol{\eta})$ as:

Preprints (www.preprints.org) | NOT PEER-REVIEWED | Posted: 16 September 2019 doi:10.20944/preprints201909.0160.v1

Peer-reviewed version available at Electronics 2019, 8, 1217; doi:10.3390/electronics8111217

$$V(Y_i) = \int_{-\infty}^{\infty} \left[\eta_i - E(Y_i)\right]^2 g_{Y_i}(\eta_i) d\eta_i \quad (4)$$

The covariance of the output quantities can be obtained by its PDF $\mathbf{g_Y(\eta)}$ as:

$$Cov(Y_i, Y_j) = Cov(Y_j, Y_i) = \int_{-\infty}^{\infty}\int_{-\infty}^{\infty} \left[\eta_i - E(Y_i)\right]\left[\eta_j - E(Y_j)\right] g_{Y_i,Y_j}(\eta_i, \eta_j) d\eta_i d\eta_j \quad (5)$$

where $g_{Y_i,Y_j}(\eta_i, \eta_j)$ is the joint PDF for the two random variables Y_i, Y_j.

The correlation of the output quantities can be obtained by its PDF $\mathbf{g_Y(\eta)}$ as:

$$Corr(Y_i, Y_j) = Corr(Y_j, Y_i) = \frac{Cov(Y_i, Y_j)}{\sqrt{V(Y_i)V(Y_j)}} \quad (6)$$

4. Experiment for determination and uncertainty evaluation of the error correction coefficients

The first experiment is the measurement of the standard artefact of the dot grid target. This experiment aims at obtaining the parameters of the coefficients of the kinematic rigid body errors. Uncertainties of the obtained correction coefficients are also evaluated.

4.1. Determination of error coefficients

The standard artefact of the dot grid target is introduced in Part I of this paper. This artefact is measured in an environment under controlled temperature of 20±1 °C, using the Leica DCM-3D Confocal Microscopy at the Metrology Laboratory of the Technical University of Madrid. A magnification objective of 50X was used, with a numerical aperture of 0.90. The acquisition parameter of measurement area was defined as the topography stitching measurement, with a 4×4 extended topographies, covering an area of 0.828×0.621 mm². The parameter of overlapping area is 25% and the correlation takes XYZ option. The level of resolution is 1, and the measured extended topographies contain 2496×1872 pixels.

After the measurement, the confocal system generated a file with suffix name '.dat', containing three vectors, which are values of X-, Y-, and Z-coordinates. Data of this file is imported and analysed by our developed algorithms. The raw measurement data is shown in Figure 2, which is an inclined surface with some outliers. This surface is aligned to be parallel with the X- and Y-coordinate plane using our developed surface rotation methods introduced in Part I. The aligned surface is shown in Figure 3. The distribution of the values of the X-, Y-, and Z-coordinates of the surface after rotation is indicated by Figure 4.

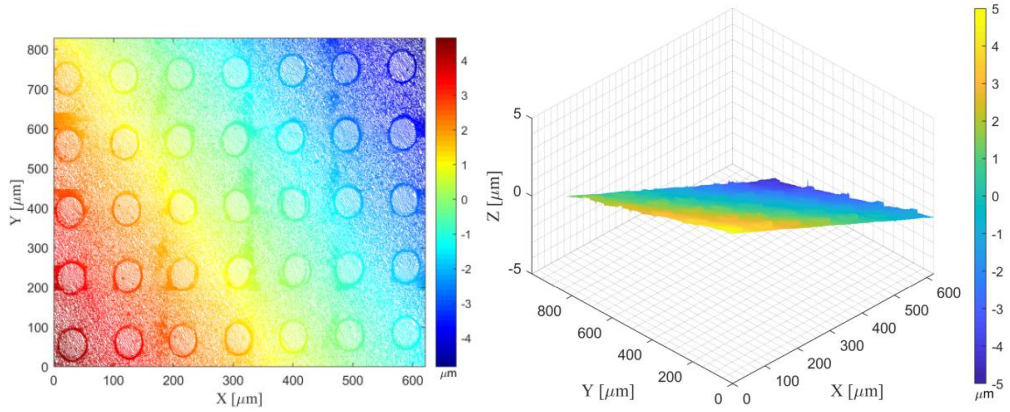

(a) (b)

Figure 2. Surface reconstruction by the raw measurement data: (a) 2D contour; (b) 3D surf.

Preprints (www.preprints.org) | NOT PEER-REVIEWED | Posted: 16 September 2019 doi:10.20944/preprints201909.0160.v1

Peer-reviewed version available at Electronics 2019, 8, 1217; doi:10.3390/electronics8111217

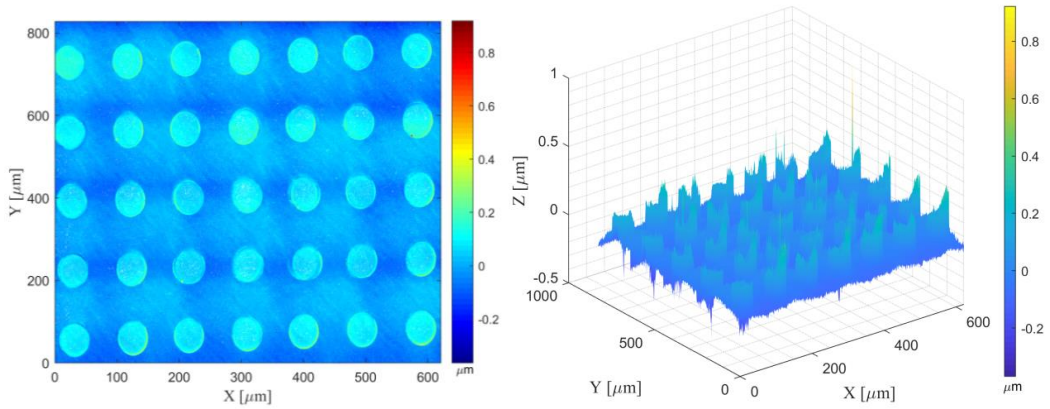

Figure 3. Surface reconstruction after rotation of the raw measured surface: (a) 2D contour; (b) 3D surf.

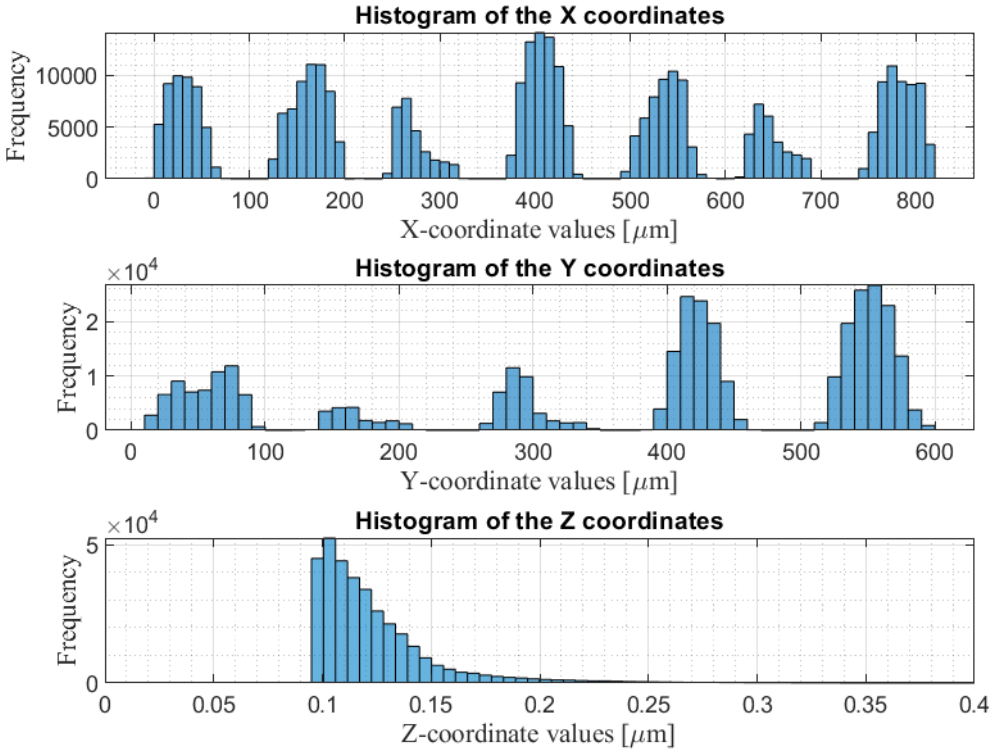

Figure 4. Histograms of the X-, Y-, and Z-coordinates of the aligned surface.

After rotation, the data is separated as surface plane and cylinders. The surface reconstruction of the data of cylinders is shown in Figure 5. It is obvious that this data has many outliers. Those outliers are detected and deleted by the method introduced in our previous work [**Error! Reference source not found.**]. The distribution of the measurement values of the X- and Y- coordinates as well as the threshold for outlier detections are shown in Figure 6 and Figure 7 individually. The surface reconstruction by the data of cylinders with outliers removed is shown in Figure 8.

Preprints (www.preprints.org) | NOT PEER-REVIEWED | Posted: 16 September 2019 doi:10.20944/preprints201909.0160.v1

Peer-reviewed version available at Electronics 2019, 8, 1217; doi:10.3390/electronics8111217

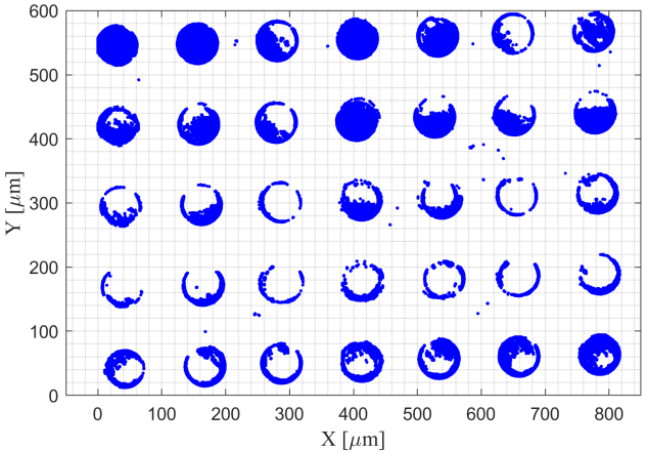

Figure 5. Surface reconstruction of the data of cylinders.

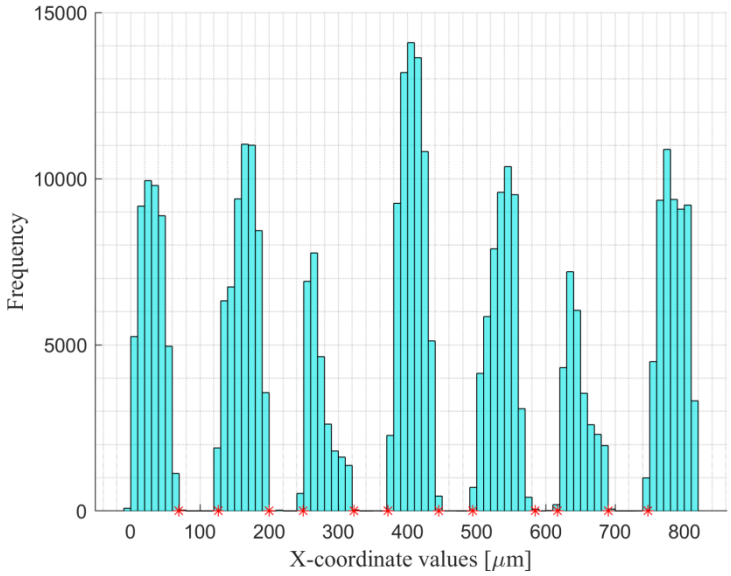

Figure 6. Distribution of the X-coordinate values and the thresholds for outlier detection.

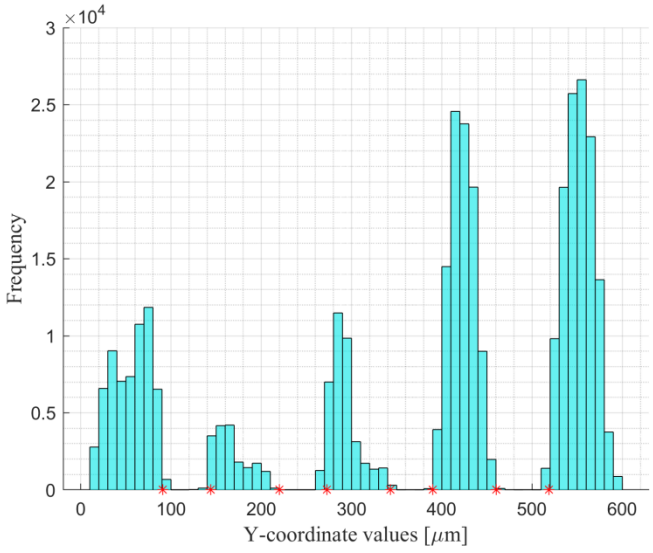

Figure 7. Distribution of the Y-coordinates values and the thresholds for outlier detection.

Preprints (www.preprints.org) | NOT PEER-REVIEWED | Posted: 16 September 2019 doi:10.20944/preprints201909.0160.v1

Peer-reviewed version available at Electronics 2019, 8, 1217; doi:10.3390/electronics8111217

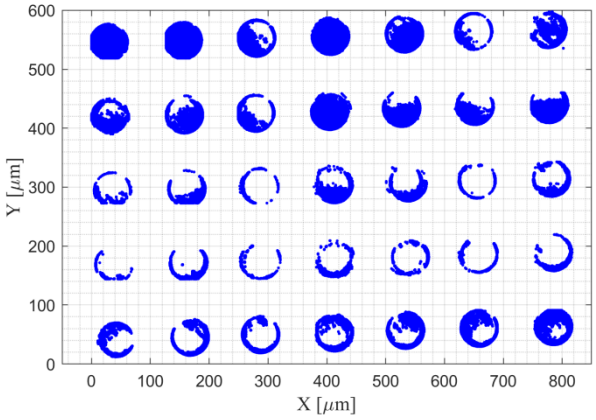

Figure 8. Surface reconstruction of the data of cylinders with outliers removed.

The separated cylinders are shown in Figure 9. They are denoted by different colours and numbers.

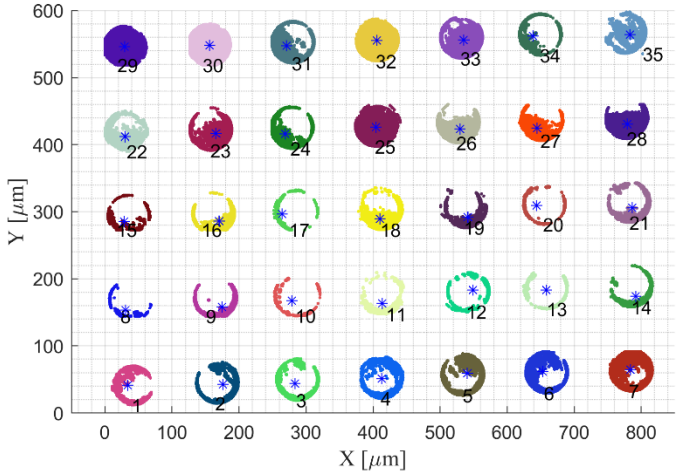

Figure 9. Separation of the cylinders.

Those individual point cloud of cylinders are processed by our introduced algorithms. Their centres are fitted and shown in Figure 10, in comparison with their corresponding certified positions.

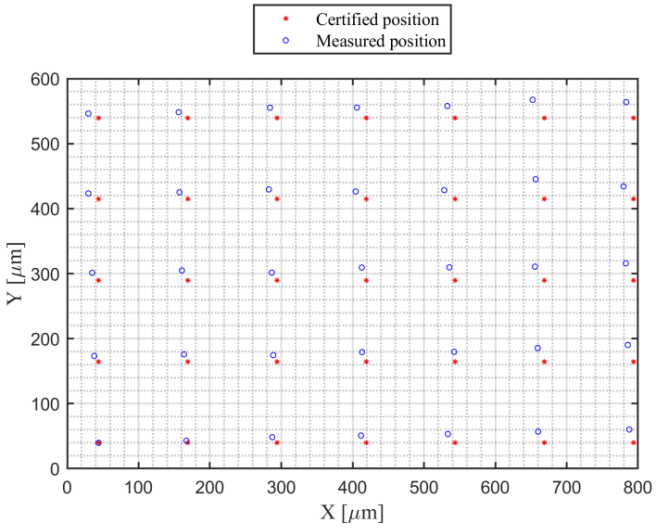

Preprints (www.preprints.org) | NOT PEER-REVIEWED | Posted: 16 September 2019 doi:10.20944/preprints201909.0160.v1

Peer-reviewed version available at Electronics 2019, 8, 1217; doi:10.3390/electronics8111217

Figure 10. Plot of the cylinders' centres and their corresponding certified positions.

It can be found that the measured cylinder centres shown in Figure 10 are all distorted in one direction. This might be caused by the location of the measurand, as it is impossible to locate the measurand parallel with the X-axis. Thereof, those measured centres are first aligned to be parallel with the X-axis. Then they are calibrated to the certified points using our developed mathematical models and algorithms. From this, the results of the coefficients defined in the mathematical model, i.e. Equations (4) and (5) in Part I, can be obtained. The results are indicated in Table 1.

Table 1. Parameters of the coefficients of the mathematical models for lateral geometric error correction.

Parameter	Value	Parameter	Value	Parameter	Value
a_1	7.38×10^{-3}	c_1	4.36×10^{-6}	e_1	6.00×10^{-6}
a_2	-1.46×10^{-6}	c_2	1.05×10^{-8}	e_2	-6.24×10^{-9}
a_3	3.19×10^{-11}	c_3	-1.20×10^{-12}	e_3	9.69×10^{-14}
b_1	1.05×10^{-3}	d_1	-7.22×10^{-3}	f_1	-2.01×10^{-2}
b_2	-1.11×10^{-5}	d_2	4.00×10^{-6}	f_2	1.25×10^{-5}
b_3	-3.15×10^{-11}	d_3	-1.01×10^{-10}	f_3	-3.10×10^{-9}

With those obtained parameters of the coefficients, the corrected points are calculated according to Equations (4) and (5) in Part I. Figure 11 shows the corresponding positions of certified, measured, and corrected points. The results of the mean errors, maximum errors, sum of squared errors, and standard deviations of the errors are indicated in Table 2.

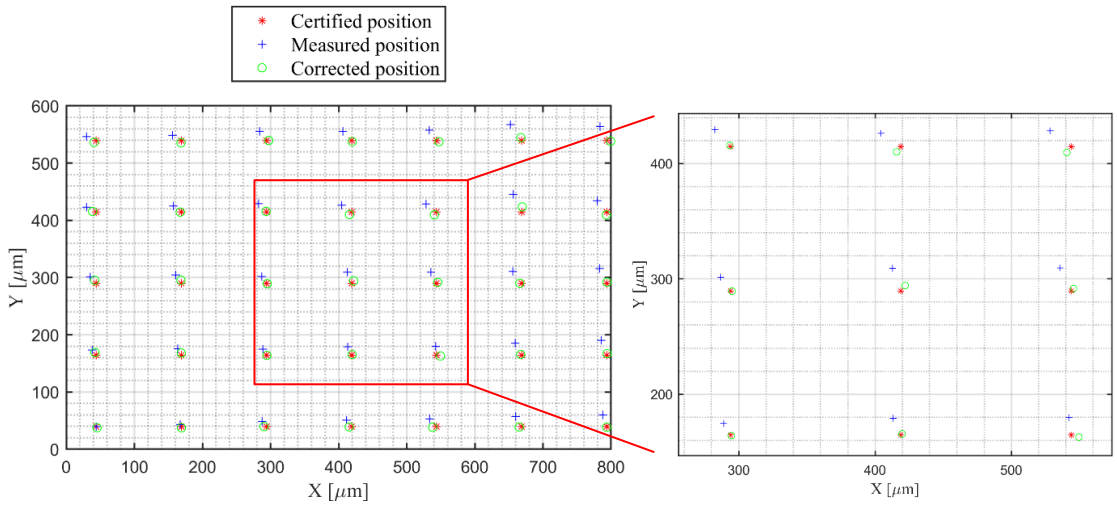

Figure 11. Comparison of the positions of certified, measured and corrected points.

Table 2. Errors with respect to the certified positions before correction and after correction.

Data types	Mean Error [μm]	Maximum error [μm]	Sum of squared errors [μm^2]	Standard deviations of the errors [μm]
Measured points	18.3	33.1	1.4×10^4	7.0
Corrected points	3.8	8.9	628.1	1.9

Peer-reviewed version available at Electronics 2019, 8, 1217; doi:10.3390/electronics8111217

The Euclidean residuals of each point are plotted by contours, as shown in Figure 12 and 13, which is the contour of the Euclidean residuals of the measured and corrected points with respect to the certified values.

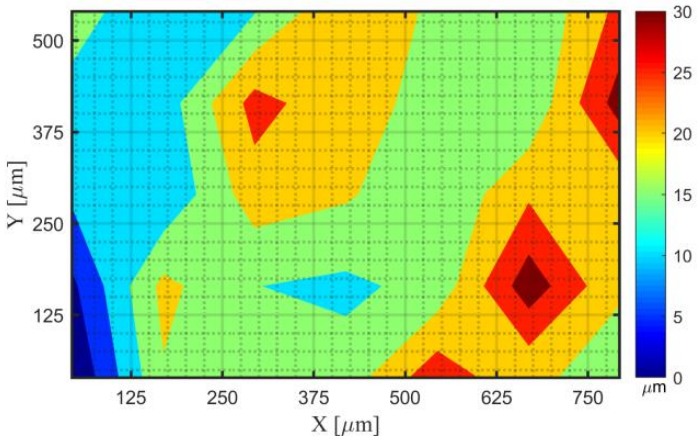

Figure 12. Contour of the Euclidean residuals between each certified and measured points.

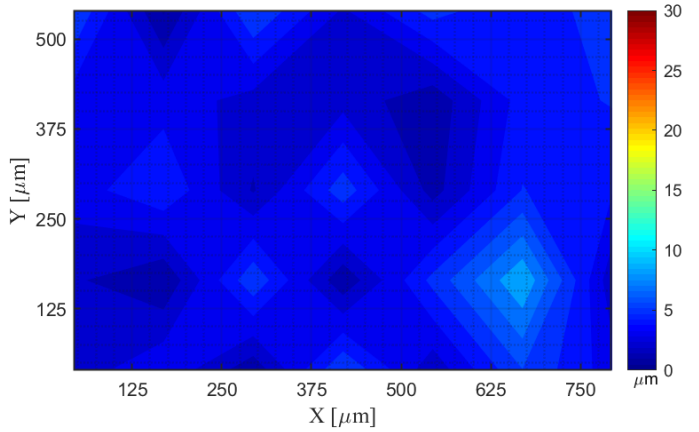

Figure 13. Contour of the Euclidean residuals between each certified and corrected points.

It can be concluded that the determined coefficients for kinematic geometric error correction works very well in this measurement.

4.2. Uncertainty evaluation

Uncertainty evaluation of the geometric error coefficients is based on the algorithms introduced in Section 3. The heart of the approach is making repeated draws from the PDFs for the input variables X_i (or joint PDF for $\mathbf{X}$) and the evaluation of the output quantity. Here defines the determinations of the number of repeated draws, namely, the number of simulation trials, the PDFs for the input variables, and the evaluation of the output quantity.

According to GUM-S2 [**Error! Reference source not found.**] the main stages of uncertainty evaluation constitute formulation, propagation, and summarizing.

I) The first stage of formulation includes:

Preprints (www.preprints.org) | NOT PEER-REVIEWED | Posted: 16 September 2019 doi:10.20944/preprints201909.0160.v1

Peer-reviewed version available at Electronics 2019, 8, 1217; doi:10.3390/electronics8111217

a) Define the output quantity, namely, the geometric error correction coefficients $\mathbf{Cc} = (a_1, ...g_3)$;

b) Determine the input quantity upon which $\mathbf{Cc}$ depends, namely, the measurement results $(\mathbf{x}, \mathbf{y})$ and their corresponded certified values $(\mathbf{P_x}, \mathbf{P_y})$;

c) Develop a measurement function f or measurement model relating the input and output quantities, namely, Equations (4) and (5);

d) On the basis of available knowledge assign PDFs to the components of the input quantities. As indicated by Table 2 in Part I, the certified values $(\mathbf{P_x}, \mathbf{P_y})$ follow a rectangular distribution $U(-1,1)$ μm. As there are no more information about the sources of uncertainties for $(\mathbf{P_x}, \mathbf{P_y})$ neither information for the measured values of X- and Y-coordinates $(\mathbf{x}, \mathbf{y})$, here does not assign more uncertainties to the input quantities, for not introducing unnecessary uncertainties.

II) The second stage is propagation:

Propagate the PDFs for the components of input quantities through the model to obtain the (joint) PDF for the output quantity.

III) The final step is summarizing:

Use the PDF for the output quantity to obtain the expectation of the output quantity, the uncertainty matrix, also named covariance matrix, associated with the expectation of the output quantity, and a coverage region containing the output quantity with a specified probability p (the coverage probability).

The simulation was repeated for 1×10^4 times. The mean values, expanded uncertainties ($k = 2$), lower and upper boundaries for a 95% coverage interval are indicated in Table 3. Distributions for the output quantities are shown in Figure 14. As it can be observed, non-symmetric distributions and not assimilable to normal distributions are obtained.

Table 3. Parameters of the coefficients of the mathematical models for lateral geometric error correction.

Parameter	Mean Value	Expanded Uncertainty	95% coverage Interval	
			Lower Boundary	Upper Boundary
a_1	7.50×10^{-3}	4.74×10^{-3}	5.07×10^{-3}	1.61×10^{-2}
a_2	-2.13×10^{-6}	5.41×10^{-6}	-1.28×10^{-5}	-6.12×10^{-8}
a_3	2.00×10^{-10}	7.14×10^{-10}	-1.35×10^{-10}	1.21×10^{-9}
b_1	-5.91×10^{-6}	8.85×10^{-3}	-1.62×10^{-2}	2.99×10^{-3}
b_2	-9.91×10^{-6}	9.19×10^{-6}	-1.50×10^{-5}	2.08×10^{-6}
b_3	-6.86×10^{-12}	2.36×10^{-9}	-8.94×10^{-10}	2.67×10^{-9}

Preprints (www.preprints.org) | NOT PEER-REVIEWED | Posted: 16 September 2019 doi:10.20944/preprints201909.0160.v1

Peer-reviewed version available at Electronics 2019, 8, 1217; doi:10.3390/electronics8111217

c_1	3.41×10^{-6}	7.89×10^{-6}	-6.22×10^{-6}	7.41×10^{-6}
c_2	1.26×10^{-8}	1.86×10^{-8}	2.21×10^{-10}	3.86×10^{-8}
c_3	-8.16×10^{-13}	3.44×10^{-12}	-5.74×10^{-12}	1.56×10^{-13}
d_1	-6.57×10^{-3}	4.97×10^{-3}	-8.53×10^{-3}	3.52×10^{-3}
d_2	3.93×10^{-6}	1.94×10^{-6}	1.39×10^{-6}	5.37×10^{-6}
d_3	-5.88×10^{-11}	3.78×10^{-10}	-4.59×10^{-10}	1.53×10^{-10}
e_1	5.89×10^{-6}	2.95×10^{-6}	2.00×10^{-6}	8.04×10^{-6}
e_2	-6.57×10^{-9}	6.71×10^{-9}	-1.44×10^{-8}	-4.88×10^{-11}
e_3	-2.34×10^{-15}	3.80×10^{-13}	-2.36×10^{-13}	3.30×10^{-13}
f_1	-2.21×10^{-2}	1.42×10^{-2}	-5.15×10^{-2}	-1.43×10^{-2}
f_2	1.40×10^{-5}	1.73×10^{-5}	6.71×10^{-6}	4.98×10^{-5}
f_3	-2.94×10^{-9}	2.92×10^{-9}	-5.37×10^{-9}	-1.14×10^{-11}

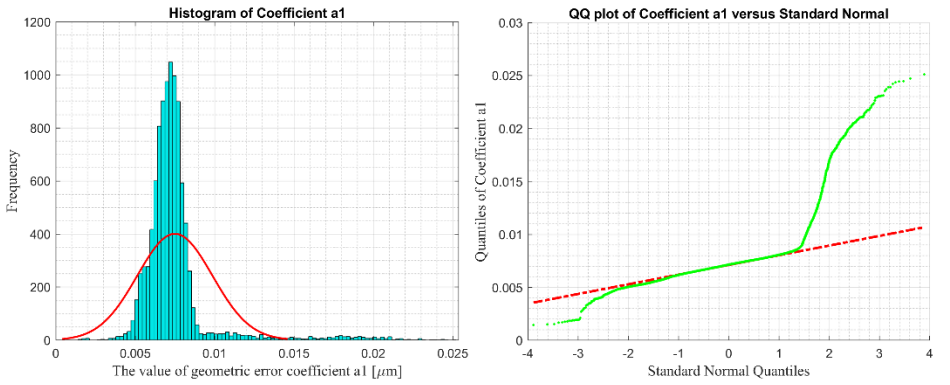

244

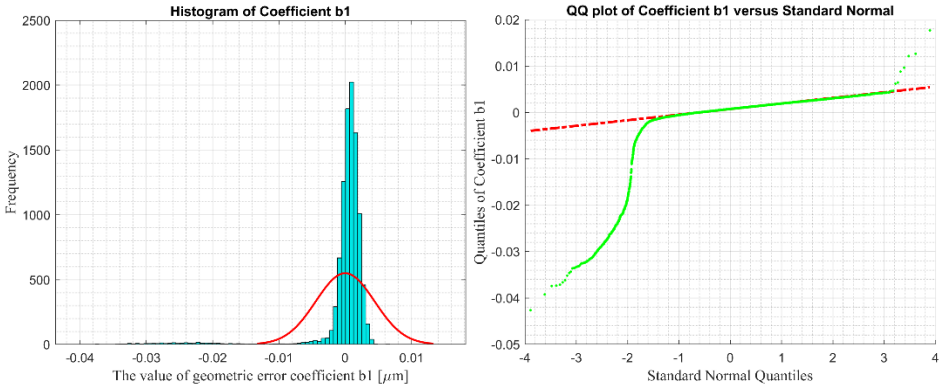

245

Preprints (www.preprints.org) | NOT PEER-REVIEWED | Posted: 16 September 2019 doi:10.20944/preprints201909.0160.v1

Peer-reviewed version available at Electronics 2019, 8, 1217; doi:10.3390/electronics8111217

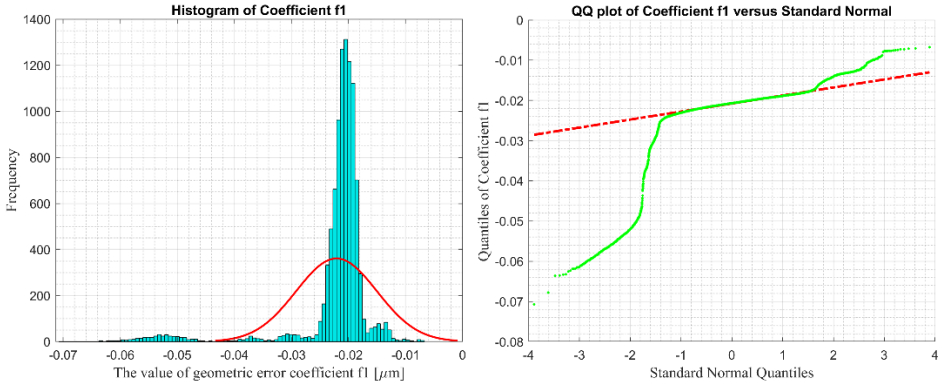

Figure 14. Distributions of the uncertainties of some geometric error correction coefficients.

5. Experimental study of the applications of determined coefficients

This section aims at verifying the applicability of the determined error correction coefficients. The residuals of measured and corrected points with respect to certified points are compared.

This experiment measures the dot grid target standard used in Section 4. The measured area of this standard is different from that in Section 4. All the environmental and operational parameters are the same with that in Section 4. The measurement data are processed using the same algorithms and procedures until the fitted cylinder centres are approximated parallel with the X-axis. Then the fitted centres are corrected by the error correction coefficients determined. By comparing the mean residuals, the sum of all squared residuals, and the standard deviation of residuals of measured points and corrected points with respect to certified positions, the effectiveness of the calculated coefficients and our model can be observed.

Measurement data are processed using our developed and validated algorithms. The raw measurement data with form removed is shown in Figure 15, implementing the form removal method presented in the pair publication Part I [18] Section 4.1. The cylinders are separated from the base with our developed algorithms, with results demonstrated in Figure 16. Figure 16 (a) shows the initial separated cylinders. Figure 16 (b) manifests the cylinders with outliers removed and with clusters classified. Figure 17 indicates the histograms of the three coordinates of the cylinders.

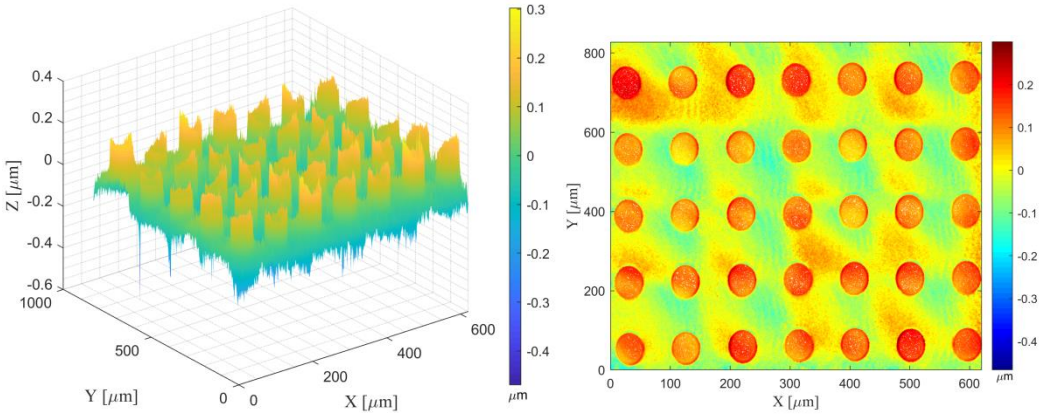

(a) (b)

Figure 15. The measured surface with form removed: (a) 3D reconstruction; (b) 2D reconstruction.

Preprints (www.preprints.org) | NOT PEER-REVIEWED | Posted: 16 September 2019 doi:10.20944/preprints201909.0160.v1

Peer-reviewed version available at Electronics 2019, 8, 1217; doi:10.3390/electronics8111217

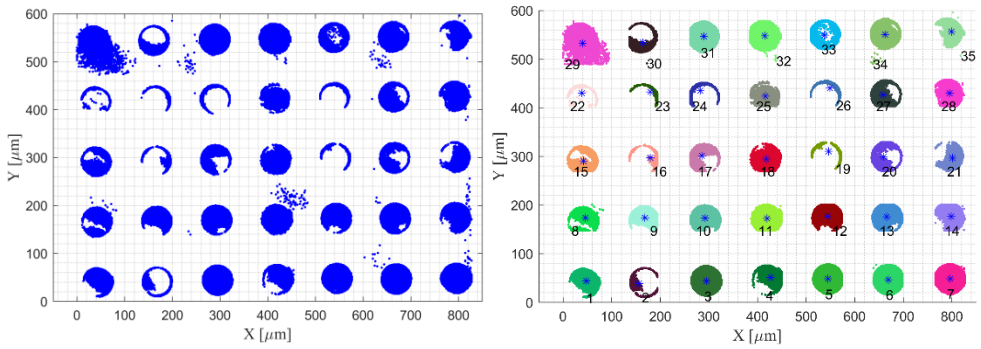

(a) (b)

Figure 16. Separation of the cylinders: (a) The separated cylinders from the base; (b) Separate cylinders into individual clusters.

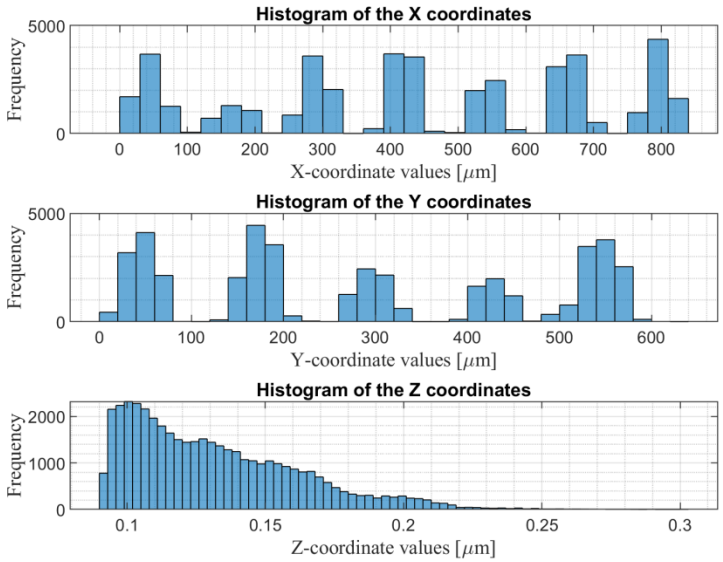

Figure 17. Histogram of the three coordinates of the separated cylinders.

The separated clusters are fitted for their centres. The coordinate values of the fitted cylinder centres are shown in Table 4. Figure 18 manifests the fitted cylinder centres as well as the centroids of each cluster data.

Table 4. The raw coordinate values of the fitted cylinder centres.

Cluster N°	X-Coordinate [μm]	Y-Coordinate [μm]	Cluster N°	X-Coordinate [μm]	Y-Coordinate [μm]
1	47.3	42.6	19	541.8	298.1
2	172.3	42.9	20	667.7	301.3
3	294.8	44.0	21	796.8	298.4
4	425.1	49.5	22	40.2	420.6
5	544.9	48.1	23	163.3	417.8
6	669.2	46.6	24	291.1	421.0
7	796.4	48.3	25	415.9	424.6
8	42.4	166.5	26	538.9	423.9
9	167.7	171.9	27	666.1	430.0
10	292.6	172.3	28	794.6	430.3
11	419.3	172.6	29	41.2	530.7
12	544.1	175.2	30	163.3	548.3

Preprints (www.preprints.org) | NOT PEER-REVIEWED | Posted: 16 September 2019 doi:10.20944/preprints201909.0160.v1

Peer-reviewed version available at Electronics 2019, 8, 1217; doi:10.3390/electronics8111217

13	666.6	174.6	31	289.5	546.6
14	797.0	176.0	32	415.0	548.2
15	40.1	295.9	33	539.9	551.7
16	163.4	294.6	34	662.6	550.7
17	293.0	294.5	35	796.9	550.8
18	417.9	295.3			

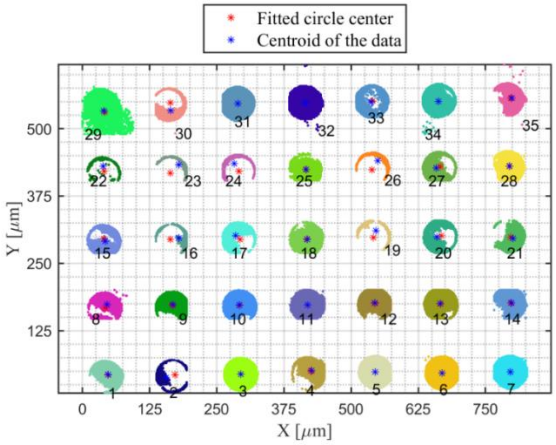

Figure 18. Comparison of the fitted circle centre and the centroid of the data.

As it can be observed in Figure 18, the cluster numbered 29 has too many outliers. Here only choose the first 28 clusters for kinematic geometric error correction. The correction employs the mathematical model Equations (4) and (5) as well as our calculated error coefficients. Before correction, the data are aligned to be parallel with the X-coordinate as much as possible. Table 5 manifests both the aligned measurement data and the corrected data.

Table 5. The aligned and corrected measurement data.

Cluster N°	Rotated measurement data		Corrected data by error coefficients	
	X-coordinate [μm]	Y-coordinate [μm]	X-coordinate [μm]	Y-coordinate [μm]
1	47.2	42.8	47.5	41.6
2	172.2	43.4	173.4	41.7
3	294.7	44.8	296.7	42.7
4	425.1	50.6	427.7	48.2
5	544.8	49.5	548.2	46.8
6	669.0	48.3	673.1	45.2
7	796.2	50.3	800.9	46.4
8	42.0	166.6	42.1	163.2
9	167.2	172.3	168.2	168.3
10	292.1	173.1	293.9	168.9
11	418.9	173.6	421.3	169.3
12	543.7	176.6	546.8	172.1
13	666.2	176.3	669.9	171.5
14	796.6	178.1	801.0	172.6
15	39.3	296.0	39.1	290.6
16	162.6	295.0	163.2	289.3
17	292.3	296.4	293.7	289.6
18	417.2	299.4	419.3	290.7
19	541.0	303.0	543.8	293.7
20	666.9	300.4	670.4	297.2
21	796.1	420.7	800.2	294.2

Preprints (www.preprints.org) | NOT PEER-REVIEWED | Posted: 16 September 2019 doi:10.20944/preprints201909.0160.v1

Peer-reviewed version available at Electronics 2019, 8, 1217; doi:10.3390/electronics8111217

22	39.1	418.2	38.6	413.4
23	162.2	418.2	162.5	410.9
24	290.0	421.7	291.1	414.6
25	414.8	425.7	416.7	418.8
26	537.9	425.3	540.4	418.6
27	665.1	431.7	668.3	425.1
28	793.5	432.2	797.4	425.5

Both the aligned and the corrected data are adjusted to a begging of $(0,0)$. The results of the measured and corrected positions are compared with the certified positions in Table 6. Figure 19 illustrates the measured, corrected, and the certified positions. The mean error, the maximum error, the sum of the squared errors, and the standard deviations of the errors are indicated in Table 7. The mean error/residual between the measured positions and the certified positions is 8.1 µm, while the mean error/residual between corrected positions and the certified positions is 5.7 µm, improved 29.6%. The maximum error between the measured positions and the certified positions is 15.6 µm, while the maximum error between corrected positions and the certified positions is 11.5 µm, reduced 26.3%. The sum of squared errors reduced from 2173.3 µm² to 1136.2 µm², which is 47.7%. It can be observed that all four types of errors are much smaller after correction with the error coefficients.

Table 6. Comparison of the certified, measured, and corrected positions.

Cluster N°	Certified position		Measured position (alignment rotated)		Corrected position	
	X-coordinate [µm]	Y-coordinate [µm]	X-coordinate [µm]	Y-coordinate [µm]	X-coordinate [µm]	Y-coordinate [µm]
1	0.0	0.0	0.0	0.0	0.0	0.0
2	125.0	0.0	125.1	0.6	125.9	0.1
3	250.0	0.0	247.6	2.0	249.2	1.1
4	375.0	0.0	377.8	7.8	380.2	6.6
5	500.0	0.0	497.7	6.7	500.7	5.2
6	625.0	0.0	621.9	5.5	625.6	3.6
7	750.0	0.0	749.1	7.5	753.4	4.9
8	0.0	125.0	-5.1	123.8	-5.4	121.6
9	125.0	125.0	120.1	129.5	120.7	126.8
10	250.0	125.0	245.0	130.3	246.4	127.3
11	375.0	125.0	371.7	130.9	373.8	127.8
12	500.0	125.0	496.5	133.8	499.3	130.5
13	625.0	125.0	619.0	133.5	622.4	129.9
14	750.0	125.0	749.4	135.2	753.5	131.0
15	0.0	250.0	-7.8	253.2	-8.4	249.0
16	125.0	250.0	115.5	252.2	115.7	247.8
17	250.0	250.0	245.1	252.5	246.2	248.0
18	375.0	250.0	370.1	253.6	371.8	249.1
19	500.0	250.0	493.9	256.6	496.3	252.2
20	625.0	250.0	619.8	260.2	622.9	255.6
21	750.0	250.0	748.9	257.7	752.7	252.6
22	0.0	375.0	-8.0	377.9	-8.9	371.8
23	125.0	375.0	115.1	375.4	115.1	369.3
24	250.0	375.0	242.9	378.9	243.7	373.0
25	375.0	375.0	367.7	382.9	369.2	377.2
26	500.0	375.0	490.7	382.5	492.9	377.0
27	625.0	375.0	617.9	388.9	620.8	383.5
28	750.0	375.0	746.4	389.5	749.9	383.9

Preprints (www.preprints.org) | NOT PEER-REVIEWED | Posted: 16 September 2019 doi:10.20944/preprints201909.0160.v1

Peer-reviewed version available at Electronics 2019, 8, 1217; doi:10.3390/electronics8111217

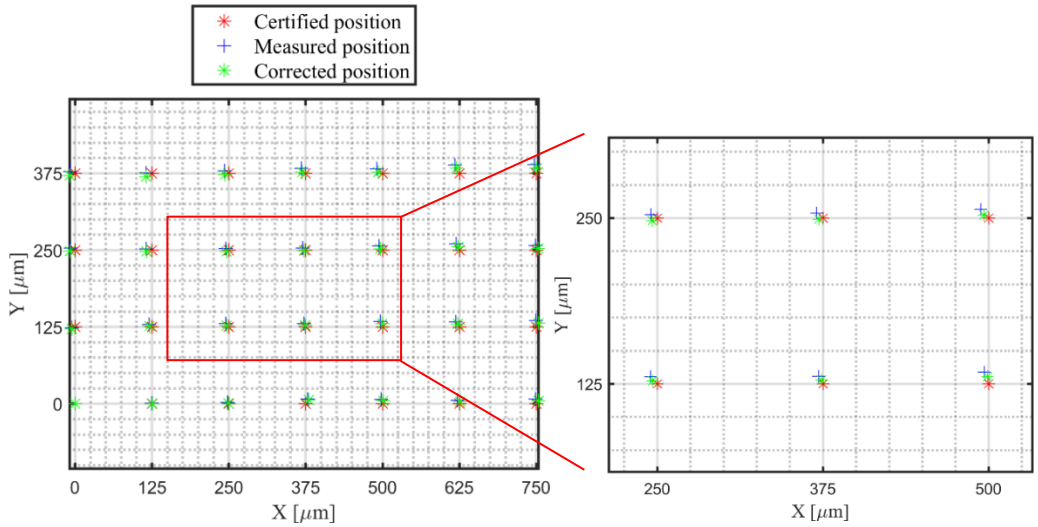

Figure 19. Comparison of the certified, measured, and corrected positions.

Table 7. Errors with respect to the certified positions before correction and after correction.

Data types	Mean Error [μm]	Maximum error [μm]	Sum of squared errors [μm²]	Standard deviations of the errors [μm]
Measured points	8.1	15.6	2173.3	3.5
Corrected points	5.7	11.5	1136.2	2.8

Figure 20 and Figure 21 manifests the contour of the mean errors of the measured data and the corrected data individually. Figure 22 compares the error vectors from the certified positons to the measured positions and the vectors from the certified positions to the corrected positions.

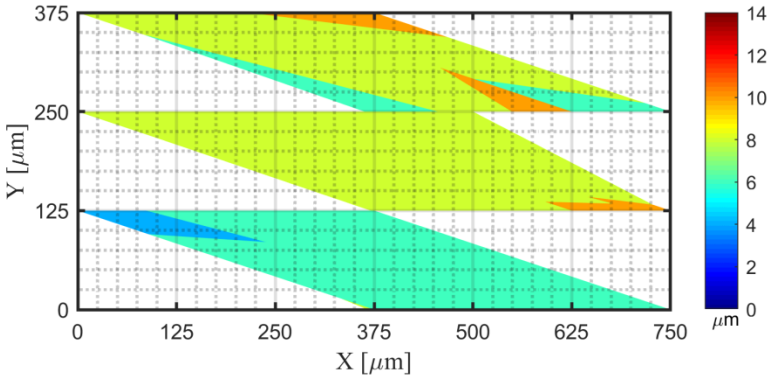

Figure 20. Contour of the Euclidean residuals between each certified and measured points.

Preprints (www.preprints.org) | NOT PEER-REVIEWED | Posted: 16 September 2019 doi:10.20944/preprints201909.0160.v1

Peer-reviewed version available at Electronics 2019, 8, 1217; doi:10.3390/electronics8111217

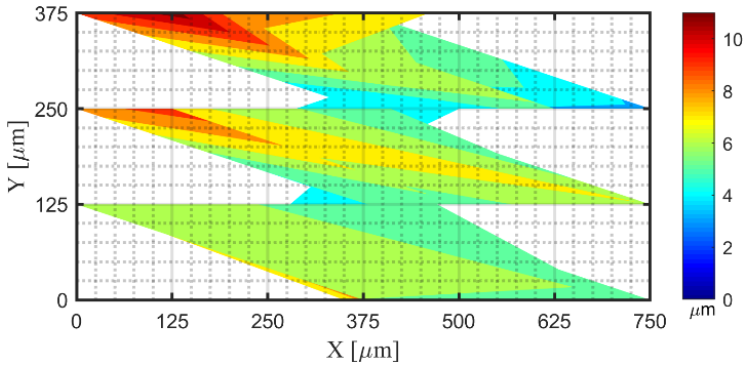

Figure 21. Contour of the Euclidean residuals between each certified and corrected points.

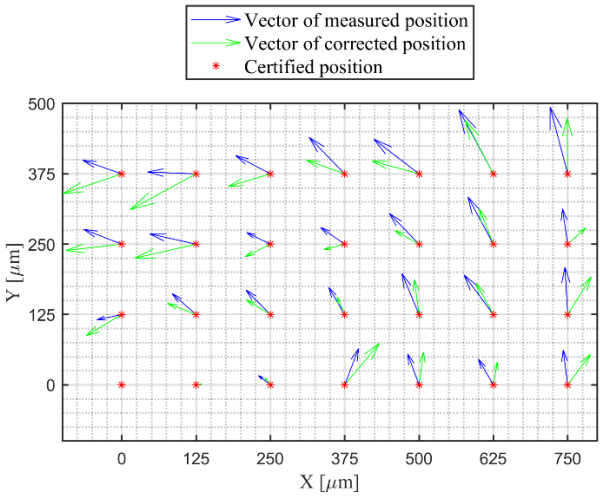

Figure 22. Comparison of the error vectors between the measured and corrected points.

According to the above results, it can be found that the errors/residuals between the corrected positions and the certified positions are much smaller than the errors/residuals between the measured positions and certified positions. This indicates that our method for the X- and Y-coordinate calibration/correction is effective and useful.

6. Conclusions and future work

This paper implemented two experiments for the illustration and the verification of our proposed method for the correction of the kinematic geometric errors produced by the movement of the lateral stage of confocal microscopes. The experimental results indicate that the mean residual reduced 29.6%, the maximum error reduced 26.3%, and the sum of squared errors reduced 47.7%.

The first experiment measured the dot grid targets with extended topography. After processing the measurement data, the error correction coefficients defined in the mathematical model, i.e. Equations (4) and (5) presented in Part I [18], were determined. The uncertainties of the values of those coefficients were also evaluated with implementation of the Monte Carlo method. The simulation number was 1×10^4. Distributions of the uncertainties of each coefficient as well as their lower and upper boundaries of a 95% interval were indicated.

The second experiment measured a different area of the same standard artefact. By correcting the measurement data using our mathematical model and the determined coefficients, the corrected results were obtained. The residuals between the raw measured points and their corresponding certified values were compared to that between the corrected points and the certified values.

The data processing algorithms and procedures, such as separations of the flats and cylinders, data partitions, outlier eliminations, K-means clustering, cylinder centres fittings, etc. were the same for both two experimental studies. The difference between the data processing for the two experiments lied in the final procedures. The first experiment fitted the values of the coefficients used non-linear Least Squared method. The second method applied the mathematical models and the determined values of the coefficients to the measured data for obtaining the corrected coordinate values of the points.

Results of the experiments demonstrated that our proposed method for lateral stage kinematic geometric error correction is efficient and useful.

Among the next practical steps for improving the proposed method is aimed at the stitching algorithm of the optical element [26], which highly needs a calibration/correction of the stitching result.

Author Contributions: Conceptualization and Methodology, C.W and E.G; Algorithms, Experiments, Data, Manuscript writing, C.W; Resources, Funding, Supervision, E.G and Y.Y; Review and Editiing, C.W, E.G and Y.Y.

Funding:This work is funded by the Spanish State Programme of Promotion of Scientific Research and Technique of Excellence, State Sub-programme of Generation of Knowledge. Project DPI2016-78476-P "Desarrollo Colaborativo de Patrones de Software y Estudios de Trazabilidad e Intercomparación en la Caracterización Metrológica de Superficies", belonging to the 2016 call for R & D Projects.
The authors acknowledge the support from the National Natural Science Foundation of China (NSFC) Project No. 51775326. the Major State Research Development Program of China (2016YFF0101905).
The authors thankfully acknowledge the Chinese Scholarship Council (CSC) for funding the first author's doctoral study.

Acknowledgement

Sincere thanks to the computer resources, technical expertise and assistance provided by the Supercomputing and Visualization Center of Madrid (CeSViMa).

Conflicts of Interests: The authors declare no conflict of interest.

References

[1] D. Jassby, T. Y. Cath, H. Buisson, The role of nanotechnology in industrial water treatment, Nature Nanotechnology (13) (2018) 670–672.

[2] T. Pfeifer, R. Freudenberg, G. Dussler, B. Brocher, Quality control and process observation for the micro assembly process, Measurement (30) (2001) 1–18.

[3] S. Bose, S. Vahabzadeh, A. Bandyopadhyay, Bone tissue engineering using 3D printing, Materials Today 16 (12) (2013) 496 – 504.

[4] K. J Stout, L. Blunt, A contribution to the debate on surface classifications - random, systematic, unstructured, structured and engineered, International Journal of Machine Tools and Manufacture 41 (13) (2001) 2039 – 2044.

[5]4. G. M. Krolczyk, J. B. Krolczyk, R. W. Maruda, S. Legutko, M. Tomaszewski, Metrological changes in surface morphology of high-strength steels in manufacturing processes, Measurement 88 (2016) 176–185.

[6] C. Wang, R. D'Amato, E. Gómez, Confidence Distance Matrix for outlier identification: A new method to improve the characterizations of surfaces measured by confocal microscopy, Measurement 137 (2019) 484 - 500.

[7] C. Wang, J. Caja, E. Gomez, Comparison of methods for outlier identification in surface characterization, Measurement 117 (2018) 312–325.

[8] F. Sekiya, A. Sugimoto, Fitting discrete polynomial curve and surface to noisy data, Annals of Mathematics and Artificial Intelligence, 75 (1-2) (2015) 135-162.

[9] B. C. T. Khac, K. H. Chung, Quantitative assessment of contact and non-contact lateral force calibration methods for atomic force microscopy, Ultramicroscopy 161 (2016) 41 – 50.

[10] P. Ekberg, L. Mattsson, Traceable X,Y self-calibration at single nm level of an optical microscope used for coherence scanning interferometry, Measurement Science and Technology 29 (3) (2018) 035005.

[11] T. Wilson, A. R. Carlini, Size of the detector in confocal imaging systems, Optics Letters 12 (4) (1987) 227–229.

[12] T. Kim, D. Gweon, J. Lee, Enhancement of fluorescence confocal scanning microscopy lateral resolution by use of structured illumination, Measurement Science and Technology 20 (5) (2009) 055501.

[13] H. Ni, L. ZOU, Q. Guo, X. Ding, Lateral resolution enhancement of confocal microscopy based on structured detection method with spatial light modulator, Optics Express 25 (3) (2017) 2872.

[14] B. Wang, L. Zou, S. Zhang, J. Tan, Super-resolution confocal microscopy with structured detection, Optics Communications 381 (2016) 277 – 281.

[15] K. Lee, J. C. Lee, S. H. Yang, The optimal design of a measurement system to measure the geometric errors of linear axes, The International Journal of Advanced Manufacturing Technology (66) (2013) 141–149.

[16] S. Ibaraki, Y. Kimura, Y. Nagai, S. Nishikawa, Formulation of Influence of Machine Geometric Errors on Five-Axis On - Machine Scanning Measurement by Using a Laser Displacement Sensor, Journal of Manufacturing Science and Engineering 137 (2) (2015) 021013.

[17] B. Daemi, P. Ekberg, L. Mattsson, Lateral performance evaluation of laser micromachining by high precision optical metrology and image analysis, Precision Engineering 50 (2017) 8 – 19.

[18] C. Wang, E. Gómez, Y. Yu, Characterization and correction of the geometric errors in using confocal microscope for extended topography measurement. Part I: Models, Algorithms Development and Validation, Electronics 8 (733) (2019).

[19] M. G. Cox, B. R. L. Siebert, The use of a Monte Carlo method for evaluating uncertainty and expanded uncertainty, Metrologia 43 (2006) S178–S188.

[20] G. Wubbeler, M. Krystek, C. Elster, Evaluation of measurement uncertainty and its numerical calculation by a Monte Carlo method, Measurement Science and Technology 19 (4pp) (2008) 084009.

[21] Evaluation of Measurement Data - Guide to the Expression of Uncertainty in Measurement (GUM).

[22] P. M. Harris, M. G. Cox, On a Monte Carlo method for measurement uncertainty evaluation and its implementation, Metrologia 51 (2014) S176–S182.

[23] JCGM 101:2008 Evaluation of measurement data - Supplement 1 to the ''Guide to the expression of uncertainty in measurement'' - Propagation of distributions using a Monte Carlo method.

[24] JCGM 102: 2011 Evaluation of measurement data - Supplement 2 to the ‘‘Guide to the expression of uncertainty in measurement” - Extension to any number of output quantities.

[25] W. Bich, M. G. Cox, R. Dybkaer, C. Elster, W. T. Estler, B. Hibbert, H. Imai, W. Kool, C. Michotte, L. Nielsen, L. Pendrill, S. Sidney, A. M. H. Veen, W. Woger, Revision of the ”Guide to the Expression of Uncertainty in Measurement”, Metrologia 49 (2012) 702–705.

[26] D. Chen, J. Peng, S. Valyukh, A. Asundi, Y. Yu, Measurement of High Numerical Aperture Cylindrical Surface with Iterative Stitching Algorithm, Applied Sciences 8 (11) (2018) 2092–2103.